

Efficient degradation of azo dyes using Ag and Au nanoparticles stabilized on graphene oxide functionalized with PAMAM dendrimers†

Cite this: *New J. Chem.*, 2014, **38**, 1551

Rajendiran Rajesh,^a S. Senthil Kumar^b and Rengarajan Venkatesan^{*a}

Received (in Montpellier, France)
4th September 2013,
Accepted 21st December 2013

DOI: 10.1039/c3nj01050c

www.rsc.org/njc

Herein, we report the stabilization of silver and gold nanoparticles (Ag/Au NPs) on graphene oxide (GO) functionalized with PAMAM dendrimers. The grafting of the PAMAM dendrimers on GO has been investigated using TGA and Raman spectral studies and the stabilization of the Ag/Au NPs on the dendritic structures has been confirmed using XRD, UV-Vis and FT-IR spectra, SEM and TEM studies. The catalytic activity of the prepared nanocatalysts towards the degradation of organic azo dyes, namely methyl orange and congo red, has been tested. The prepared nanocatalysts were found to exhibit excellent catalytic activity towards the complete degradation of both methyl orange and congo red within only a few seconds.

1. Introduction

The textile manufacturing process involves the preparation and utility of various dyes, and partly introduces these dyestuffs into aquatic systems and thus leading to environmental pollution and health hazards.^{1–5} Azo dyes have been extensively used in textile, leather and paper industries and constitute *ca.* 50% of all dyes produced and thus, the efficient degradation of azo dyes has become a challenging task for environmental chemists.⁶ Many different methodologies are being adopted to treat dye effluents, which include adsorption tactics,⁷ biological degradation,⁸ Fenton-like reactions,⁹ and photocatalysis.¹⁰ The adsorption methodology resulted in the transfer of pollutants from waste water to solid wastes and the traditionally employed biological degradation delivered a poor efficiency. In the case of Fenton-like reactions, the subsequent treatment of a ferrous slurry and also the requirement of H₂O₂ led to complexity. The thorough degradation of azo dyes is said to be achieved using photocatalysis, where the most employed photocatalytic material, TiO₂, is active only in the ultraviolet range because of its wide band gap. Immense efforts have been focused towards the modification of TiO₂ with an objective of developing visible

light-active photocatalysts, whereas their practical applications are still limited since the quantum yield is still not satisfactory.^{11,12} Thus, the development of a simple method/material for the efficient degradation of azo dyes has gained enormous significance.

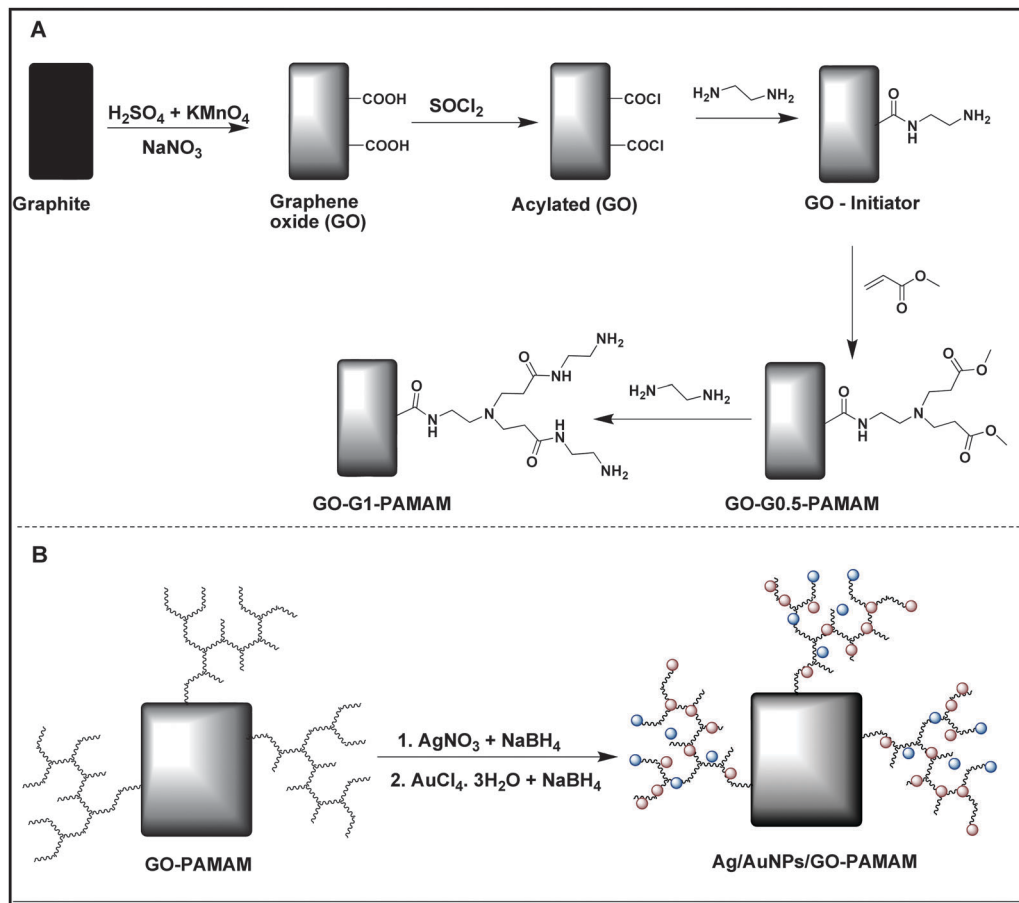
Extensive research has been carried out to explore metal nanoparticles (NPs), as they exhibit enhanced catalytic activity due to their large surface to volume ratios.^{13–15} In particular, noble metal NPs have gained more significance because of their closely packed structure and valence bands in which electrons are free to move.¹⁶ Towards the interest and progress in heterogeneous catalysis, immobilization of these metal NPs onto solid supports, that include silica,¹⁷ indium tin oxide,¹⁸ alumina¹⁹ and insoluble copolymers,²⁰ has received significant attention. However, immobilization of metal NPs into these solid surfaces tend to show less catalytic activity as a consequence of less interaction between the catalyst and the substrate. The interaction of the substrate with catalyst becomes less predominant as the catalytic sites are buried inside the solid matrix. This could be overcome by the introduction of a flexible open-arch structure on the solid support which can stabilize the metal NPs.²¹

Dendrimers are considered to be one of the most appropriate encapsulating agents for the stabilization of metal NPs due to their large size and the presence of unique three dimensional architectures of the dendrons that prevent leaching of the NPs during the course of the reaction.²² Amongst the dendrimers, (poly)amidoamine (PAMAM) dendrimers are preferable for catalytic applications because of their regular structure and chemical versatility, possessing intrinsic amino and amido functionalities. Conventional methods available for the preparation of these branched dendrimers are tedious and highly expensive. Alternatively, researchers have started grafting these dendrimers on

^a Department of Chemistry, Pondicherry University, Puducherry-605014, India.
E-mail: venkatesanr.che@pondiuni.edu.in; Fax: +91-413-2655987;
Tel: +91-413-2654415

^b Environmental & Analytical Chemistry Division, School of Advanced Sciences,
VIT University, Vellore-632014, India

† Electronic supplementary information (ESI) available: TGA data, FT-IR spectra, ¹H-NMR, SEM, TEM, surface analyser, detailed UV-Vis kinetics of the catalytic degradation of MO and CR, effect of catalytic dosage and reusability. See DOI: 10.1039/c3nj01050c



Scheme 1 Schematic illustration of the synthesis of Ag/Au NPs stabilized on GO grafted with PAMAM dendrimers. (A) Grafting of the PAMAM dendrimers on the GO surface, (B) stabilization of the Ag and Au NPs on the GO-PAMAM dendrimer support.

solid supports such as silica, CNTs, insoluble polystyrene copolymers, chitosan surfaces *etc.*, using Michael addition reactions which is extremely cost effective and also these solid supported dendrimers serve as excellent platforms for a variety of heterogeneous catalytic reactions.^{23–26}

In the present investigation, we have grafted varying branches of PAMAM dendrimers [up to three generations (G1,2,3PAMAM)] on the surface of graphene oxide (GO) followed by the stabilization of silver and gold NPs (Ag/Au NPs) on the GO supported PAMAM dendritic structure by a simple chemical reduction method (Scheme 1). Our focus here is to collectively utilize the large surface area and high electron density of GO, flexible structure of the PAMAM dendrimers and the catalytic activity of the Ag/Au NPs, towards the degradation of organic azo dyes. Ag/Au NPs stabilized on all three generations of PAMAM dendrimers (Ag/AuNPs/GO-G1,2,3PAMAM) were found to effectively degrade the dyes methyl orange and congo red, in the presence of NaBH_4 in a very short time.

2. Experimental section

2.1 Chemicals

$\text{HAuCl}_4 \cdot 3\text{H}_2\text{O}$, silver nitrate, sodium borohydride, methyl orange, congo red, potassium permanganate, hydrogen peroxide, thionyl

chloride, ethylenediamine (EDA), methacrylate (MA) were purchased from Merck, India. Graphite powder of particle size $150 \mu\text{m}$ was obtained from Sigma Aldrich. All chemicals were used without further purification. Double distilled water was used throughout the experiments.

2.2 Synthesis of Ag/Au NPs/GO-G1,2,3PAMAM

Grafting of the G1,2,3PAMAM dendrimers on GO and the stabilization of the Ag/Au NPs on the GO supported G1,2,3PAMAM was carried out using the procedure reported earlier with minor modifications.²⁷ GO was prepared based on a modified Hummers and Offeman's method.²⁸ GO (0.5 g) was dispersed in 30 mL of SOCl_2 and stirred for 24 h at 70°C and the solution was subsequently filtered and washed with anhydrous tetrahydrofuran (THF), and dried under vacuum for 24 h at room temperature, to obtain acylated GO (GO-COCl) (0.4953 g).

GO-COCl was treated with 20 mL of ethylenediamine in an ultrasonic bath (40 kHz) at 60°C for 5 h and the mixture was stirred for another 24 h. The solid obtained was separated using a $0.22 \mu\text{m}$ Millipore polycarbonate membrane filter under vacuum and then washed with anhydrous methanol. The resulting solid, after repeated washing and filtration was dried overnight under vacuum and this yielded 0.5020 g of GO-NH₂. 20 mL of methylacrylate and 50 mL of methanol were mixed in

a 250 mL three-necked round-bottomed flask to which 0.1 g of GO-NH₂ in 20 mL methanol was added dropwise within 20 min with continuous stirring. The solution was treated in an ultrasonic bath (40 kHz) at 50 °C for 7 h and the mixture was stirred for another 24 h. The filtered solid product was dispersed in methanol, filtered and then washed thrice with methanol in order to ensure that no addition free reagents were present along with the product. Then the product was dried overnight to yield GO grafted with dendrimer generation 0.5, (GO-G0.5PAMAM, 0.1011 g).

GO-G0.5PAMAM suspended in 20 mL methanol was added dropwise into 40 mL of 1:1 methanol–ethylenediamine solution. The solution was placed in an ultrasonic bath (40 kHz) at 50 °C for 5 h and the mixture was stirred for another 24 h at the same temperature. The solid was then filtered and washed with methanol thrice to yield GO grafted with dendrimer generation 1.0 (GO-G1PAMAM). The steps were repeated using methylacrylate and ethylenediamine until the desired number of generations (up to generation 3) was achieved. The dendrimer-modified GO (GO-G2,3PAMAM) were then washed thrice with methanol (25 mL), and water (25 mL) respectively.

50 mg of each GO grafted with the dendrimers of all three generations (GO-G1,2,3PAMAM), were dispersed in de-ionized water upon sonication in a 100 mL two neck round bottom flask. To each of these GO-G1,2,3PAMAM solutions, 10 mL of 0.01 M AgNO₃ solution has been added dropwise and the mixtures were stirred for 1 h. This was followed by the subsequent addition of 10 mL of 0.01 M NaBH₄ and stirring was continued for another 6 h under a nitrogen atmosphere. The obtained solid products were washed thrice with water and further dried under vacuum to yield Ag NPs/GO-G1,2,3PAMAM respectively.

Au NPs/GO-G1,2,3PAMAM were synthesized using a similar procedure. To each of the GO-1,2,3PAMAM solutions, 10 mL of 0.01 M HAuCl₄·3H₂O was added dropwise and stirred for 12 h, followed by the subsequent addition of 10 mL of 0.5 M NaBH₄ and the stirring was continued for another 24 h. The filtered solids were washed thrice with water and the products (Au NPs/GO-G1,2,3PAMAM) were dried overnight under vacuum. All the obtained nanocatalysts were insoluble in water or any other organic solvents and can be dispersed in water and other solvents upon sonication under high frequency.

2.3 Measurements

The sequence of dendrimer functionalization was monitored using a Raman spectrometer (Witec Confocal Raman instrument (CRM200) with Ar ion laser 514.5 nm). A Nicolet 6700 FT-IR spectrometer was used to record the IR spectra using the KBr pellet method. The crystalline nature of the Ag/Au NPs/GO-G1,2,3PAMAM nanocatalysts were investigated using an X-pertPRO Pananalytical X-ray diffractometer with Cu K_α radiation. The surface morphology of the Ag/Au NPs/GO-G1,2,3PAMAM nanocatalysts were analysed by SEM (HITACHI S-3400N Scanning Electron Microscope). A Tecnai F-30 field emission Transmission Electron Microscope (TEM) was employed to capture the TEM images of the Ag/Au NPs. The UV-Vis absorption spectra of the prepared nanocatalysts were recorded at room temperature with an Ocean optics (HR4000) spectrophotometer and also the catalytic activity was examined using

the same equipment. The surface area was calculated by a chem. BET pulsar TPR/TPD surface analyser.

3. Results and discussion

3.1 Covalent grafting of G1,2,3PAMAM dendrimers on GO

The functionalization of graphene oxide with PAMAM dendrimers was demonstrated in our previous report,²⁷ by investigating the weight loss of the contents using thermogravimetric analysis between 200 °C and 800 °C (ESI,† Fig. S1). Further the covalent links between PAMAM dendrimers and GO surface were verified by FT-IR spectroscopy (ESI,† Fig. S2). The formation of a GO single layer and the covalent immobilization of the G1,2,3PAMAM dendrimers on GO has been sequentially monitored by Raman spectroscopy. A laser excitation of 532 nm was employed and completely dried samples were used for measurements. The Raman spectra of pure graphite, GO-G1PAMAM, GO-G2PAMAM and GO-G3PAMAM are shown as Fig. 1 (a, b, c and d respectively). The second order 2D peak at 2732 cm⁻¹ for pure graphite in Fig. 1a is found to become increasingly diminished after each introduction step of more dendritic sites. In Fig. 1c and d, the second order 2D peaks have completely disappeared and this indicated the efficient grafting of second and third generation dendrimers on GO.²⁹ Furthermore, the Raman spectra of all the samples exhibited two predominant peaks, at 1357 cm⁻¹ and 1568 cm⁻¹, corresponding to the D and G band, respectively.^{30–33} The D and G band arise from the activation of sp³ and sp² carbons in the graphite sheets, respectively during the first order scattering process and the intensity ratio of the D to G bands expresses the sp²/sp³ carbon ratio, a measure of disorder.³⁴ In our PAMAM-grafted GO samples the D/G ratios were found to be 0.730, 0.987, 1.018, 1.03 for pure graphite, GO-G1PAMAM, GO-G2PAMAM, GO-G3PAMAM respectively, reflecting the functionalization of the PAMAM dendrimers on the GO surfaces.

3.2 Characterization of Ag/Au NPs stabilized on PAMAM dendrimer-grafted GO

The stabilization of the Ag and Au NPs on GO functionalized with PAMAM dendritic structures has been investigated by

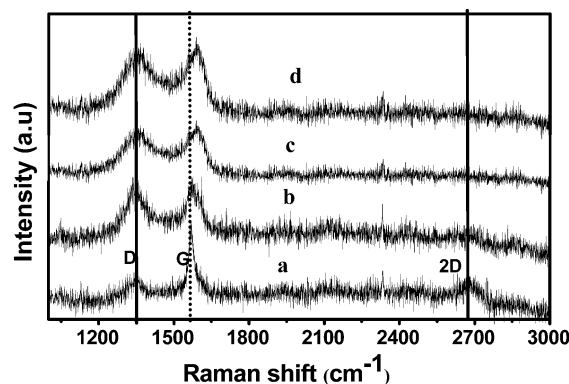


Fig. 1 Raman spectra of (a) pure graphite, (b) GO-G1PAMAM, (c) GO-G2PAMAM, (d) GO-G3PAMAM.

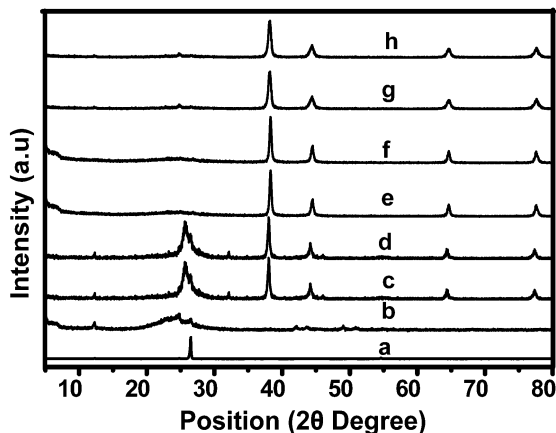


Fig. 2 The XRD patterns of (a) pure graphite, (b) GO-G3PAMAM, (c–e) Ag NPs/GO-G1,2,3PAMAM respectively, (f–h) Au NPs/GO-G1,2,3PAMAM, respectively.

comparison of their crystallinity. The X-ray diffraction patterns of pure graphite and PAMAM-grafted GO are shown in Fig. 2a and b. The diffraction pattern observed at 26.45° for pure graphite in Fig. 2a was found to disappear in Fig. 2b and this illustrates that the PAMAM-grafted graphene could be composed of mostly single or few layers. The XRD patterns in Fig. 2(c–e) at (2θ) 38.2° , 44.3° , 64.4° and 77.4° can be assigned to the (111), (200), (220) and (311) crystalline planes of Ag, respectively, and thus the Ag NPs were found to exist in the face centered cubic structure.³⁵ Similarly, the peaks observed in Fig. 2(f–h) at (2θ) 38.2° , 44.5° , 64.6° and 77.5° can be assigned to the (111), (200), (220) and (311) crystalline planes of Au, respectively, which also exists in the face centered cubic structure.³⁶ The broadening of the Bragg's peaks indicates the formation of NPs and for both Ag and Au NPs the peak corresponding to the (111) plane was more intense than the other planes, suggesting that (111) is the predominant orientation. The mean size of the Ag and Au NPs were calculated using the Scherrer formula $D = K\lambda/\beta_s \cos \theta$, where D is the average size of the particle, K is the shape dependent Scherrer's constant, λ is the wavelength of radiation, β_s is the full peak width and θ is the diffraction angle.^{37–41} Using the full width half maxima (FWHM) of the (111) peak, the size of both the Ag and Au NPs were calculated to be 20 nm, which is in good agreement with the particle size obtained from the TEM analysis.

The UV-Visible spectra of graphene oxide, GO-G3PAMAM, Ag NPs/GO-G3PAMAM and Au NPs/GO-G3PAMAM are shown in Fig. 3 (a, b, c and d, respectively). The absorbance at 240 nm in Fig. 3a is attributed to the $\pi-\pi^*$ transition of graphene oxide and the shifting of the same to 300 nm in Fig. 3b could be due to the $n-\pi^*$ transition of PAMAM dendrimer. The peaks at 417 nm and 529 nm (Fig. 3c and d) are due to the strong surface plasmon resonance characteristics of the Ag and Au NPs, respectively.^{35,38,39} The stabilization of Ag/Au NPs can also be evidenced from the FT-IR spectral investigations (Fig. S2, ESI[†]). The disappearance of peaks corresponding to NH_2 and $-\text{OH}$ functionalities in the range between of 3000 to 3050 cm^{-1} in Fig. S2c and d (ESI[†]) shows that the metal NPs are stabilized on

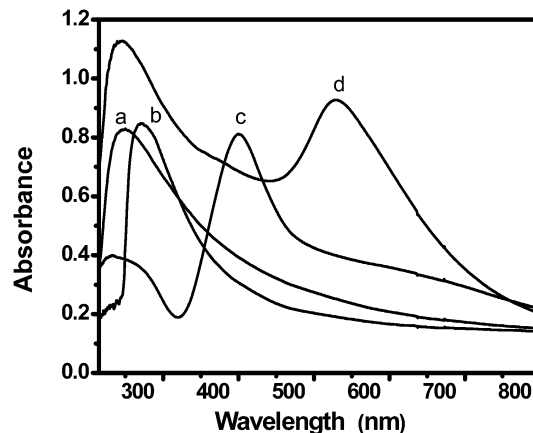


Fig. 3 UV-Visible spectrum of (a) graphene oxide, (b) GO-G3PAMAM, (c) Ag NPs/GO-G3PAMAM, (d) Au NPs/GO-G3PAMAM.

the PAMAM dendritic structures through these functional groups.

The SEM images of pure graphite (Fig. S3a, ESI[†]) shows a flake-like structure, illustrating its multi-layered morphology. In the case of the PAMAM-grafted GO shown in Fig. S3b and c (ESI[†]), the flake-like structure has collapsed into diffused snow like features and this could be due to the disruption of graphite layers upon dendrimer substitution. The SEM images of Ag NPs/GO-G1,2,3PAMAM presented in Fig. 4(a–c) are indicative of the formation of Ag NPs with a colloid-like morphology. The stabilized Ag NPs were mostly spherical in shape. Fig. 4(d–f) depicts the SEM images of Au NPs/GO-G1,2,3PAMAM and the Au NPs were also found to be spherical in shape. Unlike the Ag NP colloids, the Au NPs supported on all three generations of dendrimers were well separated and dispersed in the dendritic structure.

The surface morphology and size of the synthesized Ag/AuNPs were also examined using HR-TEM images. Fig. 5(a–c) and Fig. 5(d–f) shows the HR-TEM images of Ag and Au NPs/GO-G3PAMAM, respectively. Fig. 5(a and b) provides evidence that the Ag NPs are well dispersed across the dendritic PAMAM structures and the size of the Ag NPs has been estimated to be ~ 20 nm from Fig. 5c. The crystalline nature of the Ag NPs

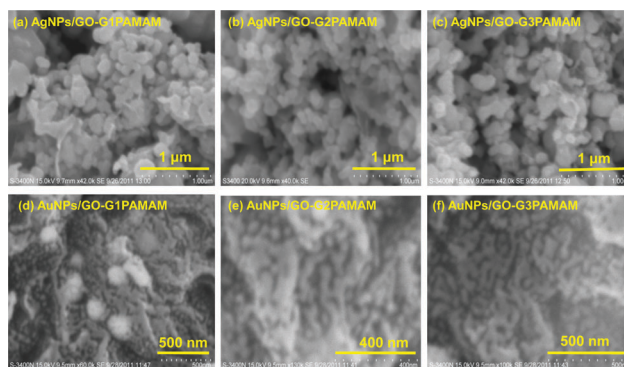


Fig. 4 SEM images of (a–c) Ag NPs/GO-G1,2,3PAMAM and (d–f) Au NPs/GO-G1,2,3PAMAM, respectively.

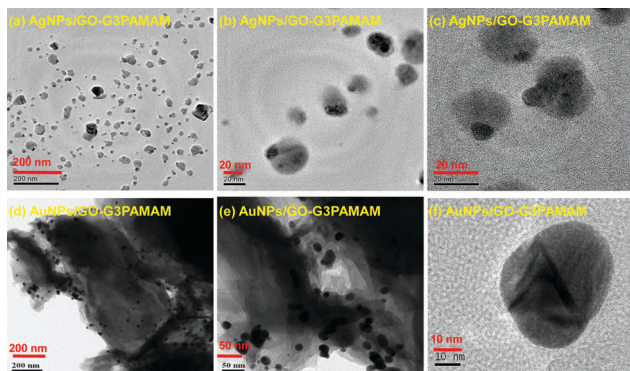


Fig. 5 TEM images of (a–c) Ag NPs/GO-G3PAMAM and (d–f) Au NPs/GO-G3PAMAM, respectively.

could not be detected by HR-TEM and this could be because of the Ag NPs being buried inside the PAMAM dendritic structure. The TEM images of Au NPs/GO-G3PAMAM shown in Fig. 5(d and e) demonstrates that the Au NPs are well dispersed across the dendritic structures and Fig. 5f showed the size of the Au NPs to be ~ 20 nm. Also the Au NPs were found to be highly crystalline and that can be observed from the lattice fringe spacing of 0.23 nm (Fig. S4a, ESI[†]), which is in agreement with that reported for the spacing between the (111) plane of fcc Au (0.235 nm) (JCPDS fill No. 04.0784), and the fringe spacing values are in accordance with that obtained from the XRD pattern of the Au NPs (Fig. 2(f–h)).^{40,41} The selected area diffraction (SAED) image of the Au NPs is presented in (Fig. S4b, ESI[†]), which shows bright diffraction rings from inner to outer, and can be indexed to the (111), (200), (220), (311) and (222) planes, respectively, confirming the highly crystalline nature of the Au NPs.³⁵

The BET surface area of pure graphite, GO, Ag NPs/GO-G1,2,3PAMAM, and Au NPs/GO-G1,2,3PAMAM were measured by nitrogen adsorption measurements and the data are depicted in Table S1, ESI[†]. The synthesized GO exhibits a significantly increased surface area ($230 \text{ m}^2 \text{ g}^{-1}$) than that of pure graphite ($8.7 \text{ m}^2 \text{ g}^{-1}$).³⁴ Interestingly, the BET surface area of the Ag NPs stabilized on GO grafted with G1,2,3PAMAM dendrimers is about $290 \text{ m}^2 \text{ g}^{-1}$, $330 \text{ m}^2 \text{ g}^{-1}$ and $365 \text{ m}^2 \text{ g}^{-1}$, respectively. Similarly Au NPs stabilized on GO-G1,2,3PAMAM have shown surface areas of $293 \text{ m}^2 \text{ g}^{-1}$, $325 \text{ m}^2 \text{ g}^{-1}$ and $358 \text{ m}^2 \text{ g}^{-1}$, respectively. The enhanced level of PAMAM dendritic structures induces the stabilization of a larger number of Ag and Au NPs, which is the origin for the gradual increase in the BET adsorption values.

3.3 Degradation of organic azo dye molecules using Ag/Au NPs/GO-G1,2,3PAMAM as heterogeneous nanocatalysts

The efficacy of Ag/Au NPs/GO-G1,2,3PAMAM nanocatalyst towards the degradation of different organic dye molecules using NaBH_4 as a reducing agent was investigated. Methyl orange (MO) and congo red (CR), which are used as commercial colorants in the dyeing industry, have been chosen as the model substrates for testing the catalytic activity of our nanocatalysts. The degradation reaction was carried out at room

temperature and the reaction was monitored with the help of an UV-Visible spectrometer. MO and CR were found to exhibit absorption maxima of 465 and 495 nm, respectively, and hence the catalytic degradation of these dyes was monitored by observing the change in absorbance of these peaks and then the pseudo-first order rate constants have been calculated.

The degradation of both MO and CR did not proceed in the absence of either NaBH_4 or the Ag/Au NPs catalysts. The degradation studies were carried out with different concentrations of NaBH_4 and Ag/Au NPs in order to optimize the suitable conditions for maximum catalytic activity. The maximum catalytic degradation was found to be attained in the presence of $50 \mu\text{L}$ of 0.1 M NaBH_4 and 5 mg of Ag/Au NPs/GO-G1,2,3PAMAM and hence the same concentration of NaBH_4 and the nanocatalysts for maintained for further investigation on the catalytic activity of Ag/Au NPs/GO-G1,2,3PAMAM. Fig. 6a and e shows the catalytic degradation of MO with time and it can be observed that complete degradation occurs within 80 s and 150 s in the presence of the Ag and Au NPs/GO-G3PAMAM nanocatalysts. Fig. 6c and g show the corresponding $\ln A$ versus time plots for the same, and the rate constants were calculated to be $25.9 \times 10^{-3} \text{ s}^{-1}$ and $19.1 \times 10^{-3} \text{ s}^{-1}$ for the degradation of MO in the presence of the Ag and AuNPs/GO-G3PAMAM nanocatalysts, respectively. Similarly, Fig. 6b and f show the degradation of CR with time in the presence of the Ag and Au NPs/GO-G3PAMAM nanocatalysts and the catalytic degradation occurs within 180 s and 240 s, respectively. The corresponding $\ln A$ vs. time plots are presented as Fig. 6d and h, and the obtained rate constant values for the reduction are $17.8 \times 10^{-3} \text{ s}^{-1}$ and $12 \times 10^{-3} \text{ s}^{-1}$, respectively. The catalytic efficiency of the Ag and Au NPs stabilized on all three generations of dendrimers has been evaluated (Fig. S5 to S8, ESI[†]) and the data are presented in Table 1. However, the NPs stabilized on the third generation dendrimers were found to exhibit the highest catalytic activity towards the degradation of both dyes, and this could be because of the presence of a higher number of metal NPs stabilized on the widely expanded third generation dendritic structures. The degradation constants calculated for all the prepared nanocatalysts towards the degradation of MO and CR were found to be comparable with or better than the reported values (Table 1). The enhanced degradation observed with our nanocatalysts can be attributed to the following reasons (i) high surface area of the GO and grafted PAMAM dendrimer that can adsorb azo dyes, (ii) NaBH_4 is expected to act as the hydride source and the Ag/Au NPs catalysts are expected to activate the azo nitrogen bond and also they could bind with the sulphur and oxygen atoms of the dyes, resulting in the weakening of the azo double bond *via* conjugation, (iii) the large number of N, O atoms of the PAMAM dendrimers could assist in increasing the number of Ag/Au NPs, and (iv) the PAMAM dendritic structures containing more hetero atoms are expected to exhibit hydrophilic interactions with the azo dyes and thus assist in bringing the dye molecules near the catalytic sites. The plausible mechanism for the degradation of MO and CR has been presented in Scheme 2 and the degradation products were characterized

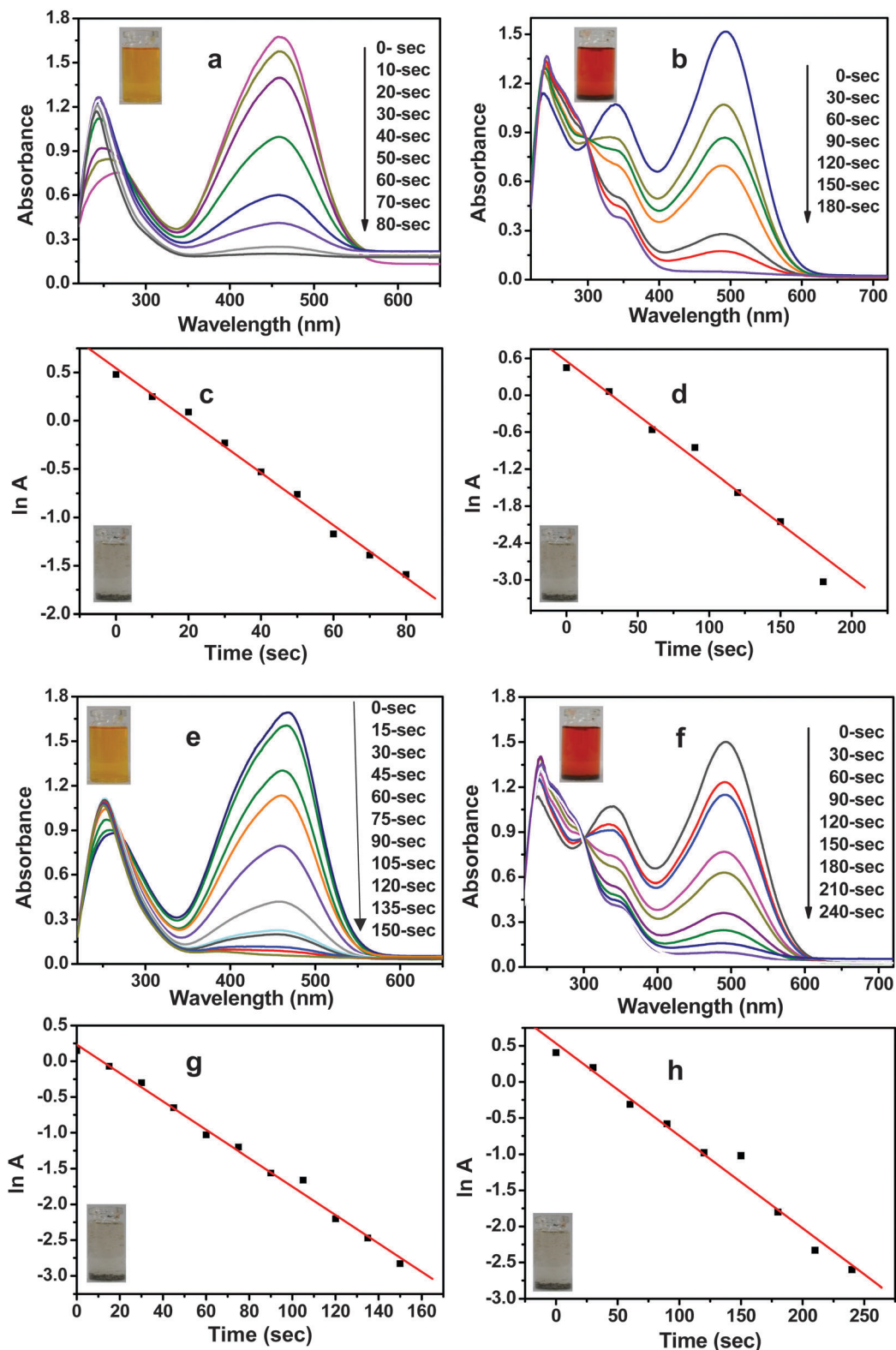


Fig. 6 UV-Vis kinetics spectra for the degradation of (a) methyl orange and (b) congo red by Ag NPs/GO-G3PAMAM. ln A vs. time plot for the degradation of (c) methyl orange and (d) congo red by Ag NPs/GO-G3PAMAM. UV-Vis kinetics spectra for the degradation of (e) methyl orange and (f) congo red by Au NPs/GO-G3PAMAM. ln A vs. time plot for the degradation of (g) methyl orange and (h) congo red by Au NPs/GO-G3PAMAM.

using NMR and FT-IR spectroscopy. Furthermore, all six catalysts could be reused at least 10 more times under similar

conditions without any change in its catalytic activity (ESI,† Fig. S25 and S26).

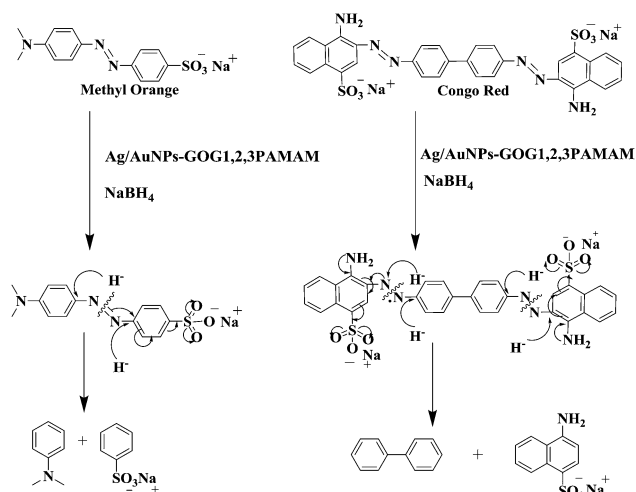
Table 1 Systematic literature survey of the degradation of methyl orange and congo red azo dyes and corresponding rate constants at room temperature

| Entry | Samples | Carrier system | Metals | Rate constants (<i>k</i>) for the degradation of | | Ref. |
|-------|--|------------------------|----------------|---|---|-----------|
| | | | | Methyl orange | Congo red ^k | |
| 1 | Ag/GO-G3PAMAM ^a | PAMAM dendrimer | Ag | $25.9 \times 10^{-3} \text{ s}^{-1}$ | $16.8 \times 10^{-3} \text{ s}^{-1}$ | This work |
| 2 | Ag/GO-G2PAMAM ^a | PAMAM dendrimer | Ag | $12.1 \times 10^{-3} \text{ s}^{-1}$ | $10.9 \times 10^{-3} \text{ s}^{-1}$ | This work |
| 3 | Ag/GO-G1PAMAM ^a | PAMAM dendrimer | Ag | $8.5 \times 10^{-3} \text{ s}^{-1}$ | $4.8 \times 10^{-3} \text{ s}^{-1}$ | This work |
| 4 | Au/GO-G3PAMAM ^b | PAMAM dendrimer | Au | $19.1 \times 10^{-3} \text{ s}^{-1}$ | $12.1 \times 10^{-3} \text{ s}^{-1}$ | This work |
| 5 | Au/GO-G2PAMAM ^b | PAMAM dendrimer | Au | $9.5 \times 10^{-3} \text{ s}^{-1}$ | $6.1 \times 10^{-3} \text{ s}^{-1}$ | This work |
| 6 | Au/GO-G1PAMAM ^b | PAMAM dendrimer | Au | $7.1 \times 10^{-3} \text{ s}^{-1}$ | $3.5 \times 10^{-3} \text{ s}^{-1}$ | This work |
| 7 | Ag/Au/Pt/tannic acid ^c | Tannic acid | Ag Au Pt | $583 \times 10^{-3} \text{ min}^{-1}$ $4.9 \times 10^{-3} \text{ min}^{-1}$ $2.9 \times 10^{-3} \text{ min}^{-1}$ | — | 42 |
| 8 | P25TiO ₂ /GO ^d | P25 | Ti | $116 \times 10^{-3} \text{ min}^{-1}$ | — | 43 |
| 9 | TiO ₂ /PW ₁₂ ^e | PAH | W | $46.5 \times 10^{-3} \text{ min}^{-1}$ | — | 44 |
| 10 | TiO ₂ /CNTS ^f | CNTS | Ti | $37.3 \times 10^{-3} \text{ min}^{-1}$ | — | 45 |
| 11 | Alumina/CuO ^g | Alumina | Cu | — | $567 \times 10^{-3} \text{ min}^{-1}$ | 46 |
| 12 | Thioacetamide/NiS ^h | Thioacetamide | Ni | — | $72 \times 10^{-3} \text{ min}^{-1}$ | 47 |
| 13 | TiO ₂ ⁱ | TiO ₂ (TNA) | Ti | — | $12.5 \times 10^{-3} \text{ min}^{-1}$ | 48 |
| 14 | P25TiO ₂ /SiO ₂ ^j | SiO ₂ | Ti | — | $0.003 \times 10^{-3} \text{ min}^{-1}$ | 49 |

^a Reactions were catalyzed by Ag NPs stabilized on GO grafted with first, second, third generation PAMAM dendrimers. ^b Reactions were catalyzed by Au NPs stabilized on GO grafted with first, second, third generation PAMAM dendrimers. ^c Tannic acid supported Ag/Au/Pt NPs. ^d Graphene oxide supported P25TiO₂ NPs. ^e Titanium oxide supported tungsten phosphate NPs. ^f Carbon nanotube supported TiO₂ NPs. ^g Alumina supported copper oxide NPs. ^h Nickel sulphate NPs. ⁱ Titanium oxide nanotube arrays NPs. ^j P25Titanium oxide supported silicone oxide NPs. ^k Apparent rate constants.

3.4 Influence of catalytic dosage

In order to examine the effect of the catalytic dosage on the rate of degradation, the reaction was carried out with varying amounts of the Ag/Au NPs/GO-G1,2,3PAMAM nanocatalysts in 1 mg increments, in the presence of an identical concentration of NaBH₄ and azo dye. It can be observed from Fig. S9–S24 (ESI[†]), that the rate of degradation increases with the amount of catalyst added up to 5 mg, and further increases in the amount of catalyst did not contribute to a significant enhancement in the degradation rate. Hence, 5 mg of the nanocatalysts has been chosen as the optimum dosage for the efficient catalytic degradation of MO and CR.



Scheme 2 Plausible mechanism for the degradation of methyl orange and congo red azo dyes by the Ag/Au NPs/GO-G1,2,3PAMAM nanocatalysts using NaBH₄ as the hydride source.

4. Conclusions

Graphene oxide grafted with PAMAM dendrimers served as an exemplary support for the stabilization of Ag and Au NPs. All the prepared nanocatalysts, Ag/Au NPs/GO-G1,2,3PAMAM were found to exhibit excellent catalytic activity towards the complete degradation of methyl orange and congo red in the presence of NaBH₄ as a hydride source, in very short reaction times. The remarkable catalytic activity achieved is attributed to the combined effect of the high surface area of graphene oxide, the highly active metal NPs and the hydrophilic dendritic structure. Furthermore, the catalysts were found to retain their activity for a high number of cycles owing to their high stability and reproducibility. These features make the Ag/Au NPs/GO-G1, 2,3PAMAM nanocatalysts good candidates for the degradation of dye pollution in water.

Acknowledgements

We gratefully acknowledge the University Grants Commission (UGC), Govt. of India, New Delhi, for funding the research project (F. No 39-782/2010 (SR)). SSK thank the Tamilnadu State Council for Science and Technology, Chennai, for the Young Scientist Visiting Fellowship. The authors also acknowledge the services rendered by the Central Instrumentation Facility (CIF), Pondicherry University.

References

- P. G. Rieger, H. M. Meir, M. Gerle, U. Vogt, T. Groth and H. J. Knackmuss, *J. Biotechnol.*, 2002, **94**, 101.
- G. M. Liu, X. Z. Li and J. C. Zhao, *Environ. Sci. Technol.*, 2000, **34**, 3982.

- 3 M. H. Habibi, A. Hassanzadeh and S. Mahdavi, *J. Photochem. Photobiol., A*, 2005, **172**, 89.
- 4 C. Hu, X. X. Hu, L. S. Wang, J. H. Qu and A. M. Wang, *Environ. Sci. Technol.*, 2006, **40**, 7903.
- 5 M. Janus and A. W. Morawski, *Appl. Catal., B*, 2007, **75**, 118.
- 6 H. Zhang, D. Chen, L. V. Xiaojun, Y. Wang, H. Chang and J. Li, *Environ. Sci. Technol.*, 2010, **44**, 1107.
- 7 J. Pengfei, J. Zhang, F. Chen and M. Anpo, *Appl. Catal., B*, 2009, **85**, 148.
- 8 F. J. Cervantes, A. G. Espinosa, M. A. Moreno-Reynosa and J. R. Rangel-Mendez, *Environ. Sci. Technol.*, 2010, **44**, 1747.
- 9 J. Fernandez, J. Bandara, A. Lopez, P. Buffat and J. Kiwi, *Langmuir*, 1999, **15**, 185–192.
- 10 J. Lee, H. S. Shim, M. Lee, J. K. Song and D. Lee, *J. Phys. Chem. Lett.*, 2011, **2**, 2840.
- 11 A. C. Pradhan, K. M. Parida and B. Nanda, *Dalton Trans.*, 2011, **40**, 7348–7356.
- 12 J. Zhang, Z. Xiong and X. S. Zhao, *J. Mater. Chem.*, 2011, **21**, 3634.
- 13 P. Kannan and S. A. John, *Electrochim. Acta*, 2011, **56**, 7029.
- 14 M. Lee, P. Amaratunga, J. Kim and D. Lee, *J. Phys. Chem. C*, 2010, **114**, 18366.
- 15 G. Chang, Y. Luo, W. Lu, X. Qin, A. M. Asiri, A. O. Al-Youbi and X. Sun, *Catal. Sci. Technol.*, 2012, **2**, 800.
- 16 D. Astruc, F. Lu and J. Ruiz Aranzaes, *Angew. Chem., Int. Ed.*, 2005, **44**, 7852.
- 17 R. Raja, V. B. Golovko, J. M. Thomas and A. B. Murcia, *Chem. Commun.*, 2005, 2026.
- 18 S. Senthil Kumar, G. Baek, S. Lee, C.-H. Jun and D. Lee, *Electrochem. Commun.*, 2012, **19**, 123.
- 19 S. Panigrahi, S. Basu, S. Praharaj, S. Pande, S. Jana, A. Pal and S. K. Ghosh, *J. Phys. Chem. C*, 2007, **111**, 4596.
- 20 B. Sreedhar, P. Surendra Reddy and D. Keerthi Devi, *J. Org. Chem.*, 2009, **74**, 8806.
- 21 Y. Jiang and Q. Gao, *J. Am. Chem. Soc.*, 2006, **128**, 716.
- 22 J. Peterson, A. Ebber, V. Allikmaa and M. Lopp, *Proc. Est. Acad. Sci., Chem.*, 2001, **50**, 156.
- 23 J. Zohuriaan and M. Mehr, *Iran. Polym. J.*, 2005, **14**, 235.
- 24 B. Pan, D. Cui, F. Gao and R. He, *Nanotechnology*, 2006, **17**, 2483.
- 25 C. Zhang, P. Su, M. U. Farooq, Y. Yang, X. Gao and E. Hongjun, *React. Funct. Polym.*, 2010, **70**, 129.
- 26 G. R. Krishnan and K. Sreekumar, *Eur. J. Org. Chem.*, 2008, 4763.
- 27 R. Rajesh and R. Venkatesan, *J. Mol. Catal. A: Chem.*, 2012, **359**, 88.
- 28 D. K. Bhui, H. Bar, P. Sarkar, G. P. Sahoo, S. P. De and A. Misra, *J. Mol. Liq.*, 2009, **145**, 33.
- 29 M. B. Avinash, K. S. Subrahmanyam, Y. Sundarayya and T. Govindaraju, *Nanoscale*, 2010, **2**, 1762.
- 30 Y. P. Sun, K. Fu, Y. Lin and W. Huang, *Acc. Chem. Res.*, 2002, **35**, 1096.
- 31 C. Cioffi, S. Campidelli, C. Sooambar, M. Marcaccio, G. Marcolongo, M. Meneghetti, D. Paolucci, F. Paolucci, C. Ehli, G. M. A. Rahman, V. S. Dirk, M. Guldi and M. Prato, *J. Am. Chem. Soc.*, 2007, **129**, 3938.
- 32 K. N. Kudin, B. Ozbas, H. C. Schniepp, R. K. Prudhomme, I. A. Aksay and R. Car, *Nano Lett.*, 2008, **8**, 36.
- 33 S. Sarkar, E. Bekyarova, S. Niyogi and C. R. Haddon, *J. Am. Chem. Soc.*, 2011, **133**, 3324.
- 34 M. Fang, K. Wang, H. Lu, Y. Yang and S. Nutt, *J. Mater. Chem.*, 2009, **19**, 7098.
- 35 D. Philip, C. Unnib, S. A. Aromala and V. K. Vidhua, *Spectrochim. Acta, Part A*, 2011, **78**, 899.
- 36 F. Bei, X. Hou, S. L. Y. Chang, G. P. Simon and D. Li, *Chem.–Eur. J.*, 2011, **17**, 5958.
- 37 S. S. Shankar, A. Ahmad and M. Sastry, *Biotechnol. Prog.*, 2003, **19**, 1627.
- 38 J. Huang, Q. Li, D. Sun, Y. Lu, Y. Su, X. Yang, H. Wang, W. Shao, N. He, J. Hong and C. Chen, *Nanotechnology*, 2007, **18**, 105.
- 39 H. Wang, X. Qiao, J. Chen and S. Ding, *Colloids Surf., A*, 2005, **256**, 111.
- 40 S. Basavaraja, S. D. Balaji, A. Lagashetty, A. H. Rajasab and A. Venkataraman, *Mater. Res. Bull.*, 2008, **43**, 1164.
- 41 G. Xu, X. Qiao, X. Qiu and J. Chen, *Colloids Surf., A*, 2008, **320**, 222.
- 42 N. Gupta, H. P. Singh and R. K. Sharma, *J. Mol. Catal. A: Chem.*, 2011, **335**, 248.
- 43 S. M. Torres, L. M. P. Martinez, J. L. Figueiredo, J. L. Faria and A. M. T. Silva, *Appl. Surf. Sci.*, 2013, **275**, 361.
- 44 P. Niu and J. Hao, *Langmuir*, 2011, **27**, 13590.
- 45 Y. J. Xu, Y. Zhuang and X. Fu, *J. Phys. Chem. C*, 2010, **114**, 2669.
- 46 D. Jana and D. Goutam, *RSC Adv.*, 2012, **2**, 9606.
- 47 H. Guo, K. Yingchang, D. Wang, K. Lin, R. Shen, J. Chen and W. Weng, *J. Nanopart. Res.*, 2013, **15**, 1475.
- 48 T. S. Natarajan, K. Natarajan, H. C. Bajaj and J. R. J. Tayade, *Ind. Eng. Chem. Res.*, 2011, **50**, 7753.
- 49 H. R. Jafry, M. V. Liga, Q. Li and A. R. Barron, *Environ. Sci. Technol.*, 2011, **45**, 1563.